Iraqi Journal of Physics, 2025
https://doi.org/10.30723/ijp.v23i3.1510

Vol. 23, No.3, PP.114-127
P-ISSN: 2070-4003
E-ISSN: 2664-5548

Calculation of Plasma Parameters for (Cu_{1-X}:Al_x) Prepared by Laser Induced Plasma: Influence Laser Energies

Nawfal A. Noori[1], Kadhim A. Aadim[1*], and Salam A. Mohammed[2]
[1]*Department of Physics, College of Science, University of Baghdad, Baghdad, Iraq*
[2]*Department of Chemical and Petroleum Engineering, College of Engineering and Agriculture, University of Nizwa, Sultanate of Oman*
[*]Corresponding author: *kadhim.aadim@sc.uobaghdad.edu.iq*
Kadhim A. Aadim is a journal editor, but he participated only as an author in the peer review process. The authors declare no other conflicts of interest

Abstract
In this work, the correlation between plasma parameters induced by pulsed laser from copper-aluminium (Cu_{1-x}:Al_x) targets at varying ratios x = 0.3, 0.5, and 0.7 and the characteristics of the ablated nanoparticles is studied, is investigated. The results show an increase in electron number density (n_e) and plasma temperature (T_e) with increasing pulsed laser energy and target ratio. The crystallite size of Cu and Al in the composite nanoparticles increased with plasma temperature from 12.4 to 17.4 nm, 13.7 to 19.1 nm, and 13.4 to 21.0 nm for Al crystallite, while it increased from 19.8 to 29.1 nm, 15.3 to 23.3 nm, and 12.3 to 18.6 nm for Cu crystallite in the x=0.3, 0.5, 0.7. The higher T_e means more energy is transferred to the plasma, which enhances the ablation process. Increasing T_e significantly increased the crystallite size of the generated nanoparticles, especially at the highest temperature. The created seed particles inside plasma may be heated by collisions with electrons, which act as a heating source during the growth of the clusters, enhancing crystallization. The crystallite size of Cu is more significant than that of Al at all laser energies for the targets from $Cu_{0.7}$:$Al_{0.3}$ and $Cu_{0.5}$:$Al_{0.5}$, and is opposite at the $Cu_{0.3}$:$Al_{0.7}$ sample. The difference in crystallite size between the two elements in the composite nanoparticles depends on their presence in the target and the pulsed laser energy, resulting from the differing capabilities of laser interaction with the other elements.

Article Info.

Keywords:
PLA, Plasma Characteristics, OES, Cu:Al NPs, Structural Properties.

Article history:
Received: Aug. 09, 2025
Revised: Aug. 24, 2025
Accepted Aug. 25, 2025
Published:Sep. 01,2025

1. Introduction
There are several approaches for evaluating plasma characteristics. Optical emission spectroscopy (OES) is most commonly utilized due to its simplicity and accuracy, and it does not affect the plasma, unlike internal probes [1]. The OES technique involves analyzing the electromagnetic radiation emitted by excited atoms and ions within the plasma [2,3]. Beyond providing insights into plasma characteristics, OES also facilitates the determination of the ionization degree [4]. Spectroscopic analysis offers valuable information on plasma behavior and composition, with particular emphasis on the interactions between the sputtering target material, the working gas, and the kinetic energy distribution of plasma species [5]. This method elucidates the interactions of atoms and ions in terms of both their energy and concentration [6]. The study of plasma properties by spectroscopy is of great importance in the real-time monitoring of nanoparticle formation during laser ablation [7] and in atomization systems, as the plasma components and their kinetic properties are essential because they are directly related to the dynamics of different species [8], which affect the properties of the prepared nanoparticles [9].

This technique can be used to fine-tune the properties of the generated nanoparticles for specific requests from various scientific fields [10-11]. The control of properties is achieved by tuning them. This work aims to identify a correlation between characteristics obtained during

the ablation process of copper: aluminum target of different composition ratios using various pulsed laser energy. Optical emission spectroscopy is utilized to characterize the induced plasma at different conditions correlated with the prepared nanoparticles' structural properties.

2. Experimental Setup

Laser-induced Breakdown Spectroscopy (LIBS) was employed in this study. It comprises a laser source and an optical emission spectrometer. The Nd: YAG laser (Diamond-288 Pattern EPLS) of fundamental wavelength 1064 nm with varying pulsed energy 400, 500, 600, 700, and 800 mJ was utilized for plasma induced. A power supply provided an external handheld piece of the pulsed laser; The laser intensity and spot size were adjusted by altering the distance between the laser lens and the target. The Nd: YAG laser is focused onto the target using a convex quartz lens with a focal length of 10 cm.

Spectral diagnostics were taken during the ablation process from Cu:Al targets at different mixing ratios, which monitored the plasma characteristics using the emission intensity of the laser- induced plasma to determine plasma parameters. A spectrometer (Thorlabs- CCS 100/M) of a high resolution $\Delta\lambda < 0.5$ nm was used to capture the emissions spectra of the plasma plume over a wavelength range from 200 to 1000 nm, which was collected by an optical fiber positioned at an angle of 45° to the laser beam axis and then directed onto the entrance slit of the spectrometer.

The prepared nanoparticles were tested using X-ray diffraction (XRD) on a SHIMADZU-6000 diffractometer with an X-ray tube emitting Cu-Kα radiation of monochromatic wavelength $\lambda = 1.5405$ Å, an applied voltage of 40 kV, and a current of 30 mA, with a step size of 0.05 degrees. The X-ray scanning was performed between 2θ values within the diffraction angle range of 20-80°.

3. Results and Discussions

Figs. (1, 2, and 3) illustrate the spectroscopic patterns of plasma induced by pulsed laser at different pulsed energies from Cu: Al targets to varying weight ratios of $Cu_{0.7}$:$Al_{0.3}$, $Cu_{0.5}$:$Al_{0.5}$, and $Cu_{0.3}$:$Al_{0.7}$ targets, respectively. The observed emissions were matched with characteristic atomic and ionic reference lines for copper and aluminum electronic transitions (Cu I, Cu II, Al I, and Al II) from the NIST site [12]. The variations in emission intensity across different wavelengths were attributed to differences in transition probabilities and statistical weights associated with each transition, as determined by the plasma temperature, according to the Boltzmann distribution [13, 14].

Notably, the evidence of emission intensities corresponding to ionic species exhibited a higher degree of ionization levels due to using a pulsed laser. Emission line intensity increased with increasing the laser pulsed energy from 400 to 800 mJ, which corresponded to more excitation with more photons by the increased laser energy. Notably, the variation in lines intensity corresponding to the different targets with varying Cu:Al ratios is consistent with the Boltzmann distribution, where higher temperatures favored a larger population of particles in higher energy states, resulting in more intense emission lines [15]. Furthermore, comparing the three figures revealed distinct trends in emission lines where the line corresponding to the Al increased with increasing its content in the targets.

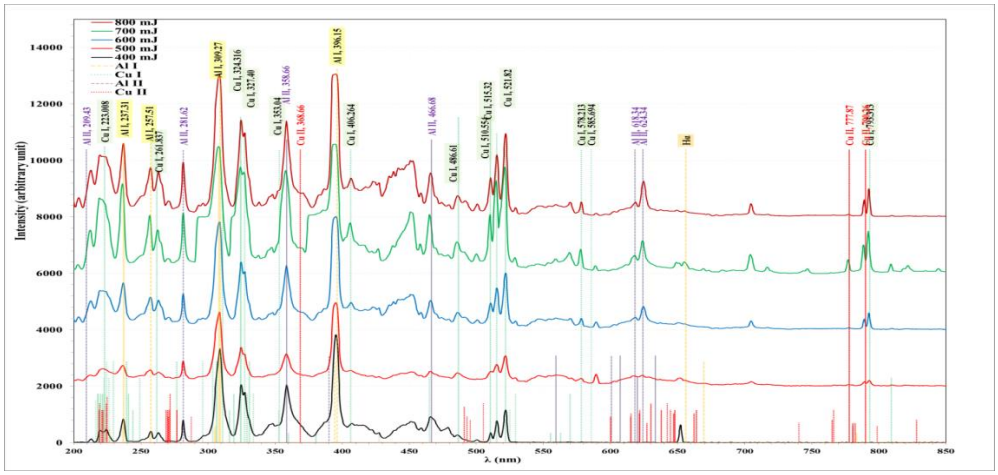

Figure 1: Emitted spectra for LIBS from $Cu_{0.7}$:$Al_{0.3}$ target using different laser pulsed energies.

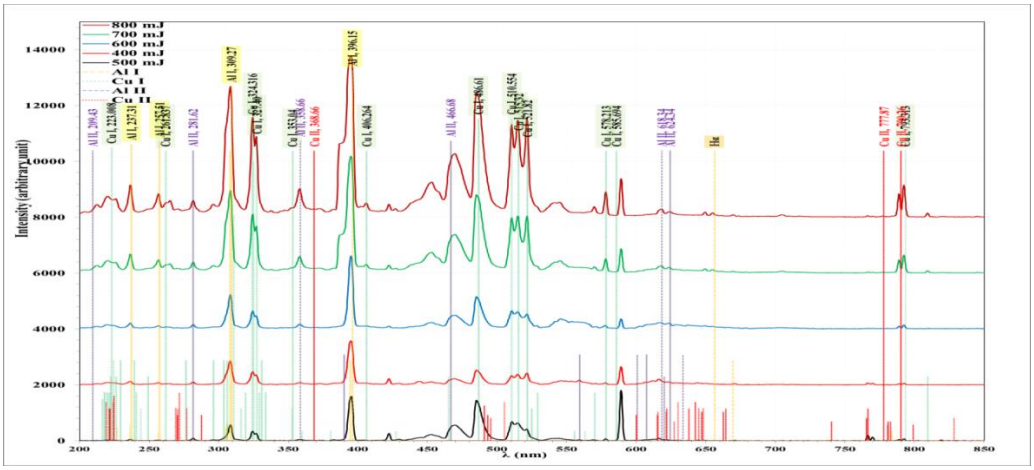

Figure 2: Emitted spectra for LIBS from $Cu_{0.5}$:$Al_{0.5}$ target using different laser pulsed energies.

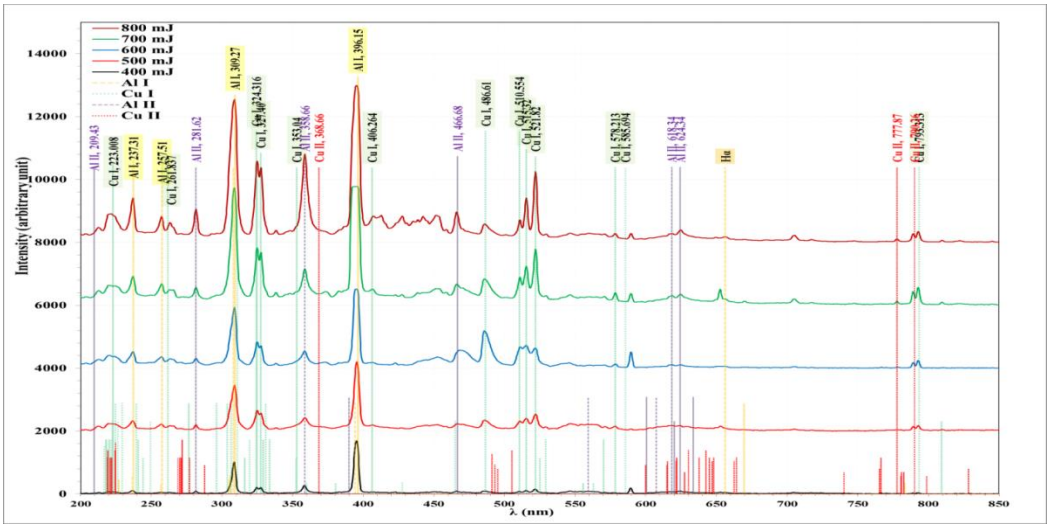

Figure 3: Emitted spectra for LIBS from $Cu_{0.3}$:$Al_{0.7}$ target using different laser pulsed energies.

Fig. 4 illustrates the variation in intensity ratio for the selected emission lines Al-I (309.27 nm)/ Cu-I (324.75 nm) from the three targets Cu:Al at different mixing ratios. The observed ratio of emission lines responds to variation in the pulsed laser energy and the Cu: Al target ratio. It is seen that that high intensity ratios greater than unity (especially the high ratio at low laser energy)

indicate the higher intensity of the Al line than for Cu as a result of the lower work function of Al than Cu, 4.3 and 4.7 eV, respectively [16]. The metal's work function can influence the intensity of plasma emission induced by pulsed laser irradiation. The work function refers to the energy required to extract an electron from the surface of a material. When a metal surface is exposed to a pulsed laser, the photons can excite electrons within the metal, causing them to be ejected from the surface and forming plasma. The work function is crucial in determining how easily electrons can be liberated from the metal surface [17]. Metals with lower work functions require less energy to release electrons, so that they may exhibit stronger plasma emission under the same laser conditions than metals with higher work functions.

Additionally, the work function can impact the efficiency of processes such as photoemission and thermal emission, which contribute to plasma formation. At lower laser energies, the limited energy available for interaction makes the difference in work functions more pronounced. This results in a higher intensity ratio of aluminum emission lines than copper. As the energy of the pulsed laser increases, both metals can interact more efficiently with it. Conversely, the intensity ratio of Al/Cu increased as predicted with increasing Al content in the target.

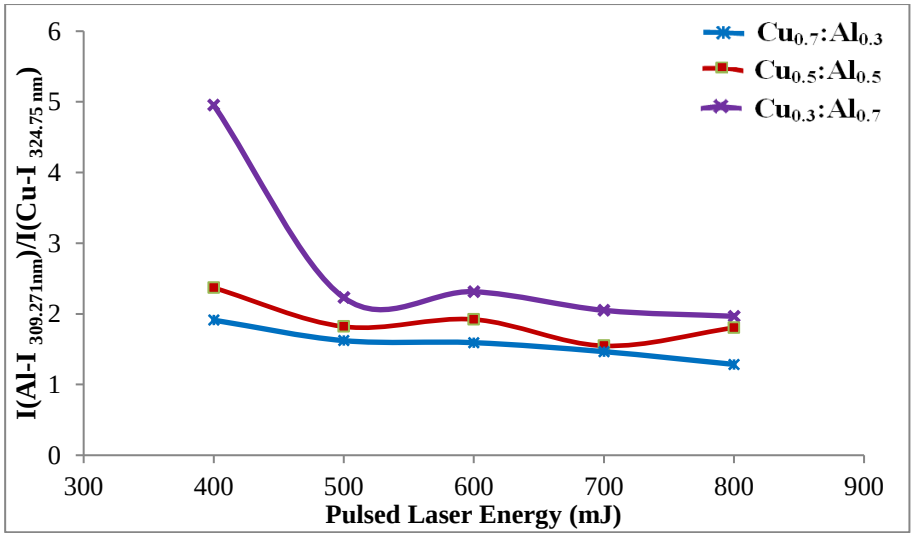

Figure 4: variation of intensity ratio for emission lines Al-I (309.27)/Cu-I (324.75 nm) from the three mixed targets Cu: Al at different mixing ratios with pulsed laser energy.

The Boltzmann-Plot was employed to determine the electron temperature (T_e) using the emission lines of Al I species at different pulsed energy onto $Cu_{0.7}$:$Al_{0.3}$, $Cu_{0.5}$:$Al_{0.5}$, and $Cu_{0.3}$:$Al_{0.7}$ targets as shown in Figs. (5, 6, and 7), respectively. The linear relationship of Ln (λjiIji/ hcAji.gj) against the upper-level energy (Ej) was plotted. The presence of high R^2 values signifies an excellent line fitting.

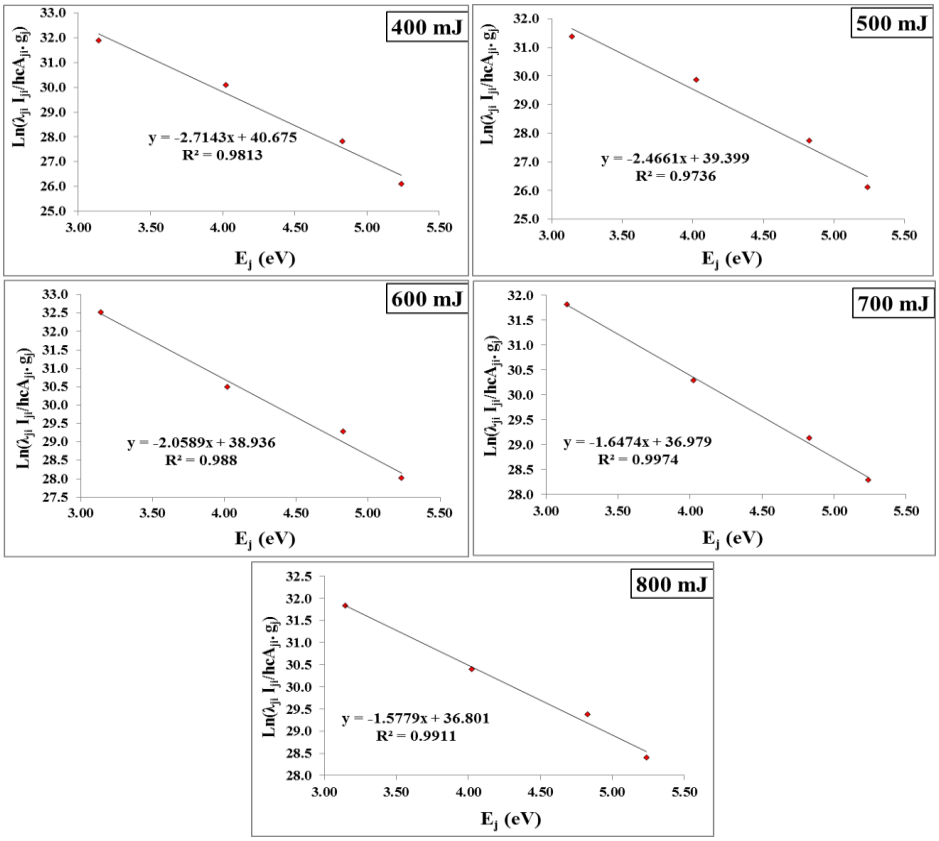

Figure 5: Boltzmann-plot using Al-I plasma emission lines using LIBS from $Cu_{0.3}$:$Al_{0.7}$ target using different laser pulsed energies.

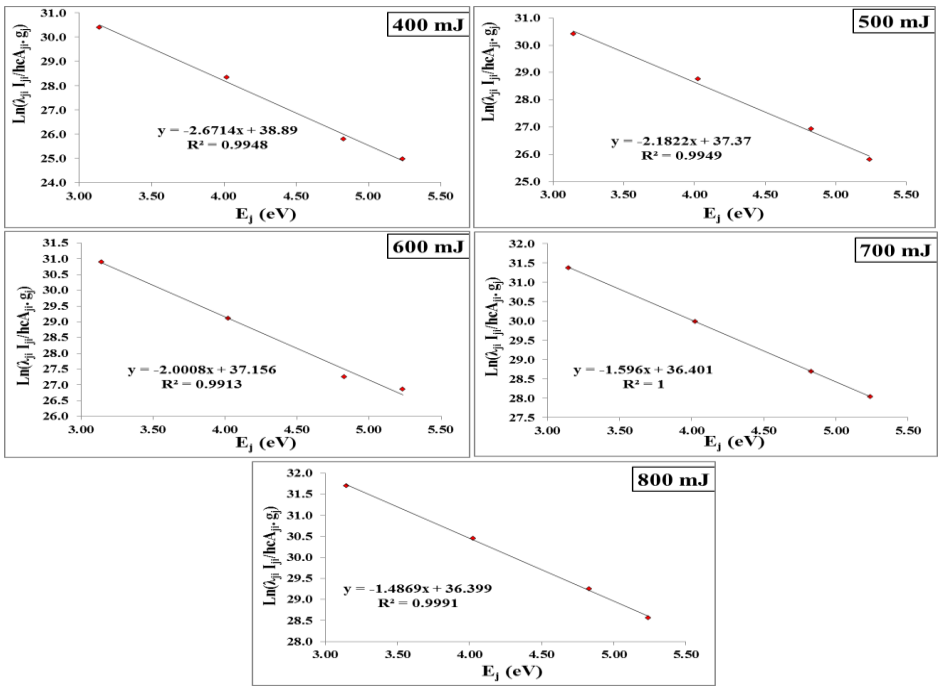

Figure 6: Boltzmann-plot for Al-I plasma emission lines using LIBS spectra from $Cu_{0.5}$:$Al_{0.5}$ target using different laser pulsed energies.

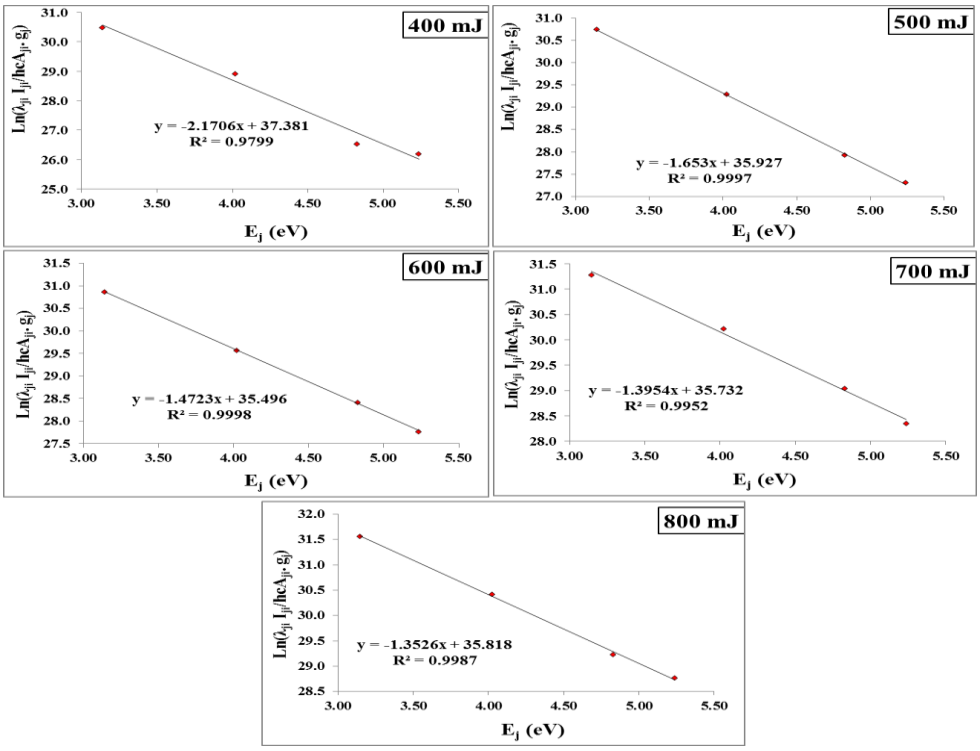

Figure 7: Boltzmann-plot for Al-I plasma emission lines using LIBS from $Cu_{0.3}$:$Al_{0.7}$ target using different laser pulsed energies.

Figs. (8, 9, and 10) illustrate the Lorentzian fitting for emitted Al II, 281.62 line for LIBS from the three Cu: Al targets at different ratios using different laser pulsed energies. A preference for fitting emission line profiles with Lorentzian curves over other profiles, such as Gaussian curves, can depend on various factors, including the nature of physical processes and the characteristics of the observed data. If the broadening of emission lines is primarily due to mechanisms such as natural or Stark broadening, which result in symmetric line shapes, Lorentzian curves are often more appropriate. Lorentzian functions naturally account for these broadening mechanisms and provide a better representation of the observed line shapes. The predominant influence of Stark broadening compared to other types of broadening often allows for neglecting these other mechanisms when determining plasma density. Consequently, line broadening varies with laser energy and target material type, reflecting changes in plasma density [18].

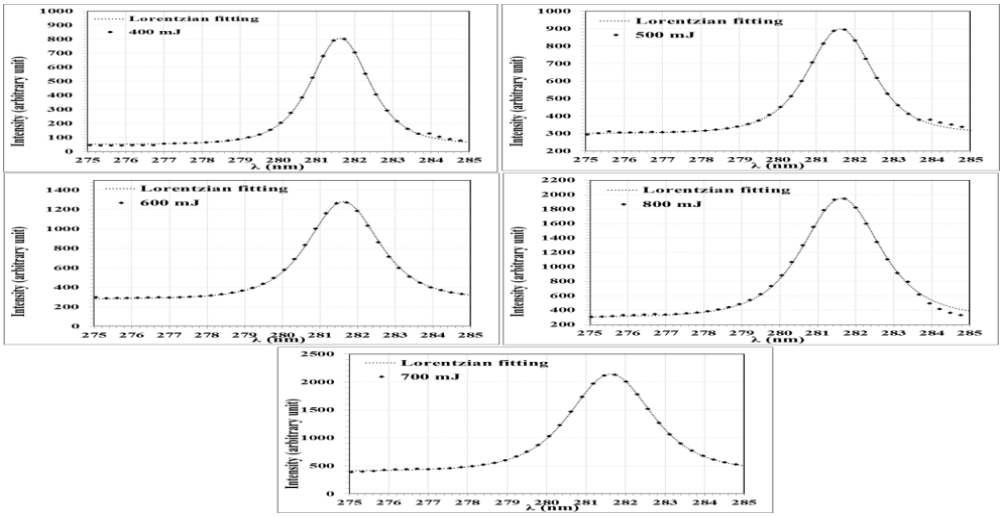

Figure 8: Lorentzian fitting for emitted Al II, 281.62 line for LIBS from $Cu_{0.7}$:$Al_{0.3}$ target using different laser pulsed energies.

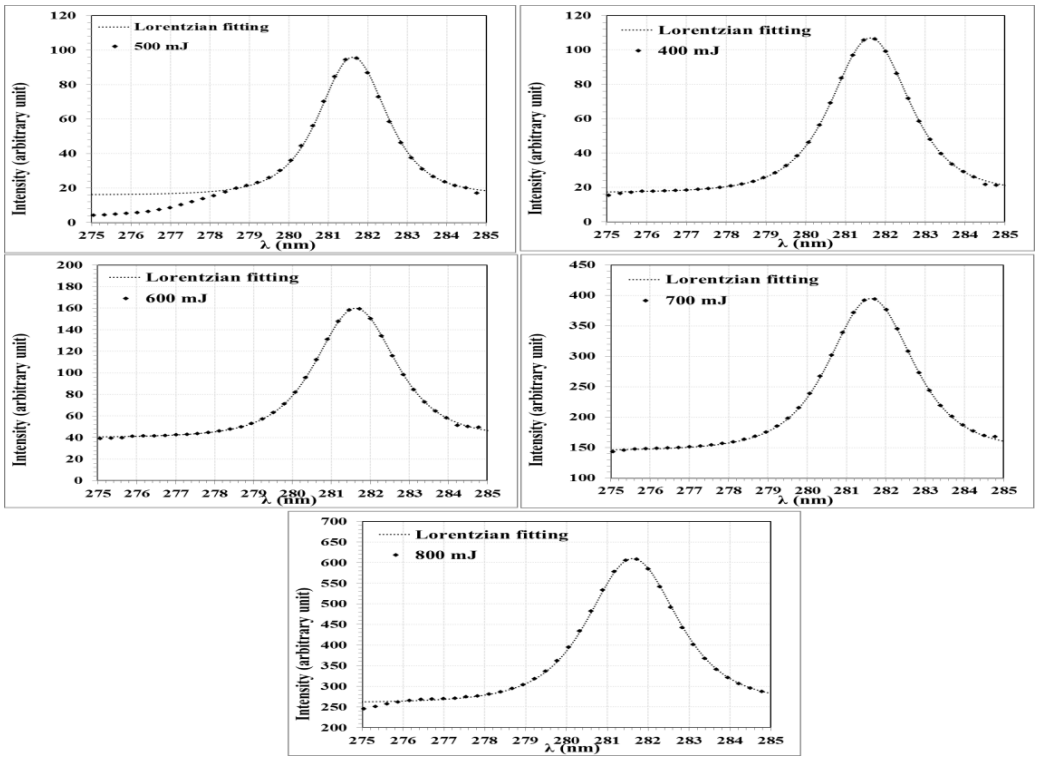

Figure 9: Lorentzian fitting for emitted Al II, 281.62 line for LIBS from $Cu_{0.5}$:$Al_{0.5}$ target using different laser pulsed energies.

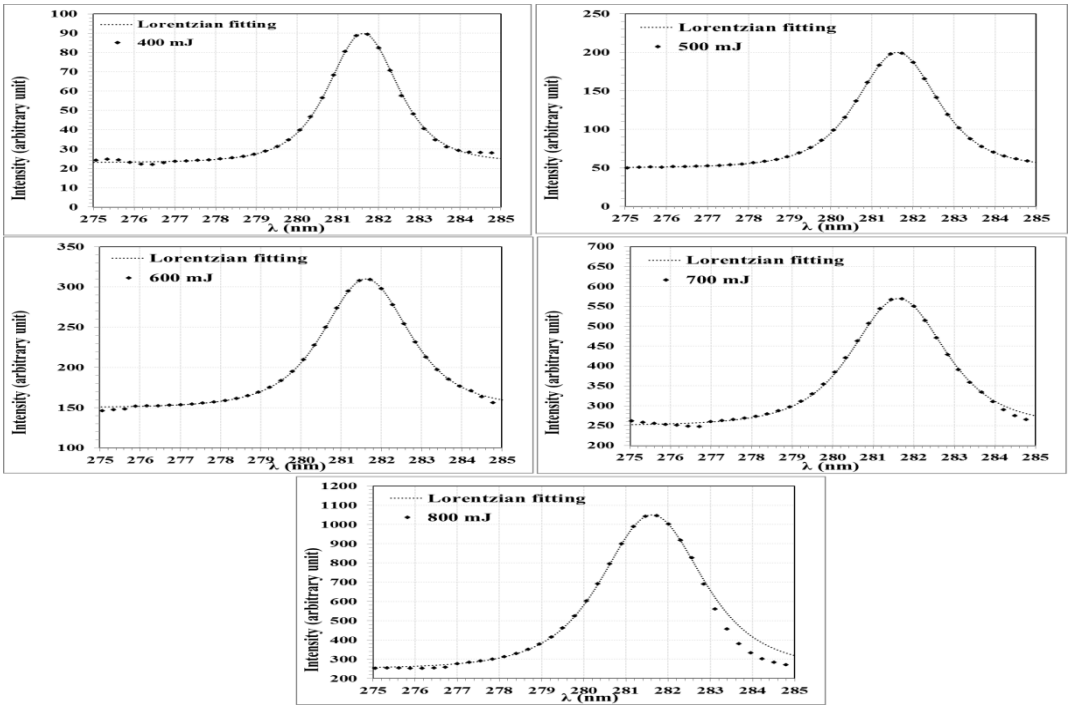

Figure 10: Lorentzian fitting for emitted Al II, 281.62 line for LIBS from $Cu_{0.3}$:$Al_{0.7}$ target using different laser pulsed energies.

Table 1 lists the plasma parameters induced by the pulsed laser from Cu: Al targets at different mixing ratios using different pulsed laser energies (400-800 mJ). These parameters vary according to the pulsed laser energy and change slightly with the target ratio. The plasma parameters meet the plasma criteria, including a high plasma frequency, a short Debye length, and a large Debye number. In general, both T_e and n_e increase the pulsed laser energy by increasing the energy delivered to the electrons, leading to growing n_e and ionization collisions.

On the other hand, both T_e and n_e slightly increase with the increase in the Al ratio in the Cu:Al targets, due to the variation in the interaction between the laser beam and the target surface, which has different absorbance capabilities according to the target composition. Concurrently, the plasma frequency displays behaviour consistent with the electron number density, as it directly correlates with the square root of the electron number density. The variation in λ_D is in line with the change in pulsed laser energy.

Table 1: plasma parameters for LIBS from the three Cu: Al targets at various mixing ratios using different laser pulsed energies.

Sample	E (mJ)	T_e (eV)	$\Delta\lambda$ (nm)	$n_e \times 10^{18}$ (cm^{-3})	$f_p \times 10^{12}$ (Hz)	$\lambda_D \times 10^{-6}$ (cm)	N_D
$Cu_{0.7}$:$Al_{0.3}$	**400**	0.368	1.800	2.123	13.083	3.095	264
	500	0.405	2.000	2.358	13.791	3.081	289
	600	0.486	2.200	2.594	14.464	3.215	361
	700	0.607	2.400	2.830	15.107	3.441	483
	800	0.634	2.450	2.889	15.264	3.480	510
$Cu_{0.5}$:$Al_{0.5}$	**400**	0.374	2.000	2.358	13.791	2.960	256
	500	0.458	2.300	2.712	14.789	3.054	324
	600	0.500	2.400	2.830	15.107	3.122	361
	700	0.627	2.500	2.948	15.419	3.425	496
	800	0.673	2.550	3.007	15.572	3.514	546
$Cu_{0.3}$:$Al_{0.7}$	**400**	0.461	2.300	2.712	14.789	3.062	326
	500	0.605	2.500	2.948	15.419	3.366	471
	600	0.679	2.700	3.184	16.024	3.432	539
	700	0.717	2.800	3.302	16.318	3.462	574
	800	0.739	2.800	3.302	16.318	3.516	601

Figs. (11, 12, and 13) illustrate the XRD patterns of the prepared composite NPs using different pulsed laser energies from the three Cu: Al targets at various weight ratios of $Cu_{0.7}$:$Al_{0.3}$, $Cu_{0.5}$:$Al_{0.5}$, and $Cu_{0.3}$:$Al_{0.7}$, respectively. All patterns appeared as polycrystalline structures of Cu and Al structures in addition to a minor CuO phase due to some oxidization at the surface of nanoparticles. The diffraction peaks appeared at different intensities according to their composition existence and the laser energy. The diffraction lines corresponding to the Cu seemed to have higher intensities than those for Al due to the association of XRD with the atomic weight and low sputtering [19].

The higher intensity of Cu diffraction lines compared to Al could be attributed to the higher atomic scattering factor and stronger X-ray interaction of Cu compared to Al, leading to more diffraction peaks and the higher relative crystallinity of Cu in the composite material compared to Al [20]. Increasing the Al content causes an increase in the diffraction peaks corresponding to the Al compared with the Cu. The diffraction line broadening varies with the laser energy and the target composition ratio. The variation of target composition causes variation in the energy absorption efficiency. So, increasing the Al content causes an increase in the crystallinity of Al but not linearly due to the different reflectivity and absorption of laser energy of the targets [21,22].

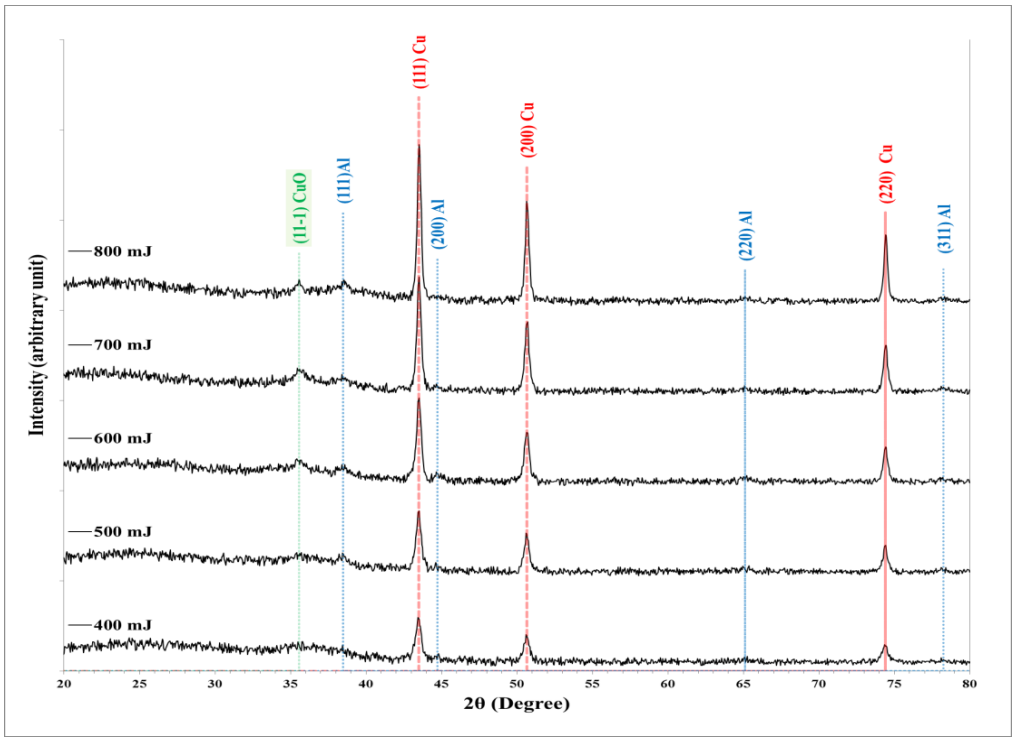

Figure 11: XRD of the prepared composite NPs from $Cu_{0.7}$:$Al_{0.3}$ target using different pulsed laser energies.

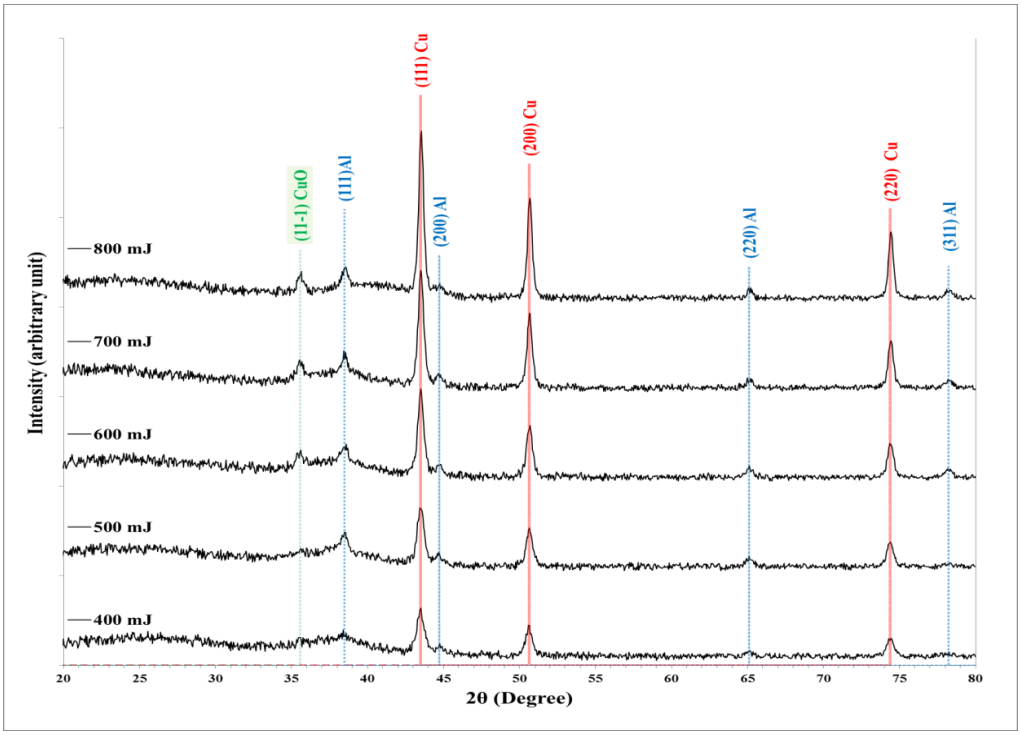

Figure 12: XRD of the prepared composite NPs from $Cu_{0.5}$:$Al_{0.5}$ target using different pulsed laser energies.

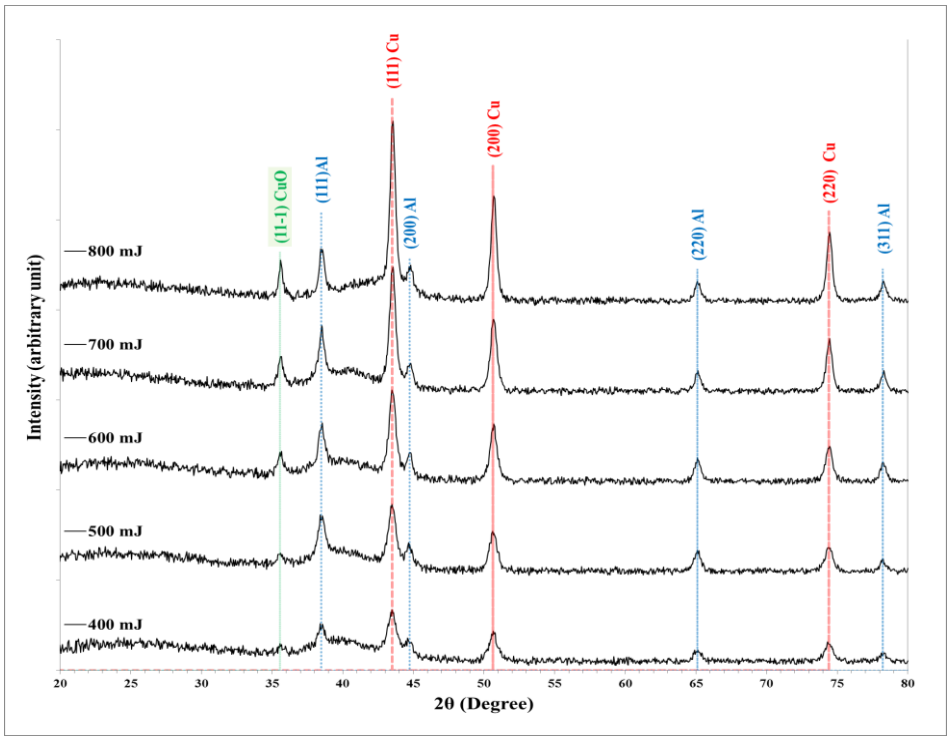

Figure 13: XRD of the prepared composite NPs from $Cu_{0.3}$:$Al_{0.7}$ target using different pulsed laser energies.

The interplanar spacing (d_{hkl}) was determined according to the Bragg formula [23]

$$n\lambda = 2d_{hkl}\sin\theta \qquad (1)$$

where (θ) is the diffraction angle, λ is the x-ray wavelength, and n is the diffraction order. The crystallite size was determined using Debye-Scherer formula [24]

$$D = \frac{0.9\,\lambda}{\beta\,.\cos(\theta)} \qquad (2)$$

where β is the breadth of the diffracted line at half maxima (in radian).

Table 2 lists the 2θ, dhkl, and D values corresponding to the preferred orientation (111) of Al and Cu structures from the three Cu:Al targets at various mixing ratios using different laser pulsed energies.

Table 2: XRD parameters corresponding to the preferred orientation of Al and Cu structures from the three Cu: Al targets at various mixing ratios using different laser pulsed energies.

Sample	Pulsed Energy (mJ)	Al (111)			Cu (111)		
		2θ (Deg.)	d_{hkl} (Å)	D (nm)	2θ (Deg.)	d_{hkl} (Å)	D (nm)
$Cu_{0.3}:Al_{0.7}$	**400**	38.4470	2.3395	12.4	43.4733	2.0800	19.8
	500	38.4632	2.3386	12.5	43.4853	2.0794	21.2
	600	38.4752	2.3379	13.9	43.4973	2.0789	23.6
	700	38.4872	2.3372	15.5	43.5093	2.0783	26.2
	800	38.4992	2.3365	17.4	43.5213	2.0778	29.1
$Cu_{0.5}:Al_{0.5}$	**400**	38.4660	2.3379	13.7	43.4843	2.0795	15.3
	500	38.4742	2.3379	13.7	43.4963	2.0789	17.0
	600	38.4862	2.3372	15.3	43.5083	2.0784	18.9
	700	38.4982	2.3365	17.0	43.5203	2.0778	21.0
	800	38.5102	2.3358	19.1	43.5323	2.0773	23.3
$Cu_{0.3}:Al_{0.7}$	**400**	38.4732	2.3380	13.4	43.4953	2.0790	12.3
	500	38.4852	2.3373	15.1	43.5073	2.0784	13.6
	600	38.4972	2.3366	16.5	43.5193	2.0779	15.1
	700	38.5092	2.3359	18.7	43.5313	2.0773	16.8
	800	38.5212	2.3352	21.0	43.5433	2.0768	18.6

Fig.14 shows the variation of crystallite size of copper and aluminium crystals, calculated using the Scherrer formula, with laser energy from different Cu: Al ratios of the targets. The crystallite size increased as the laser energy increased, which resulted in more ablated substance being produced from the target. On the other hand, the crystallite size of the two metals in the created composite nanoparticles depends on their existence in the target, where the crystallite size of Cu decreased and Al increased with increasing the Cu: Al ratio.

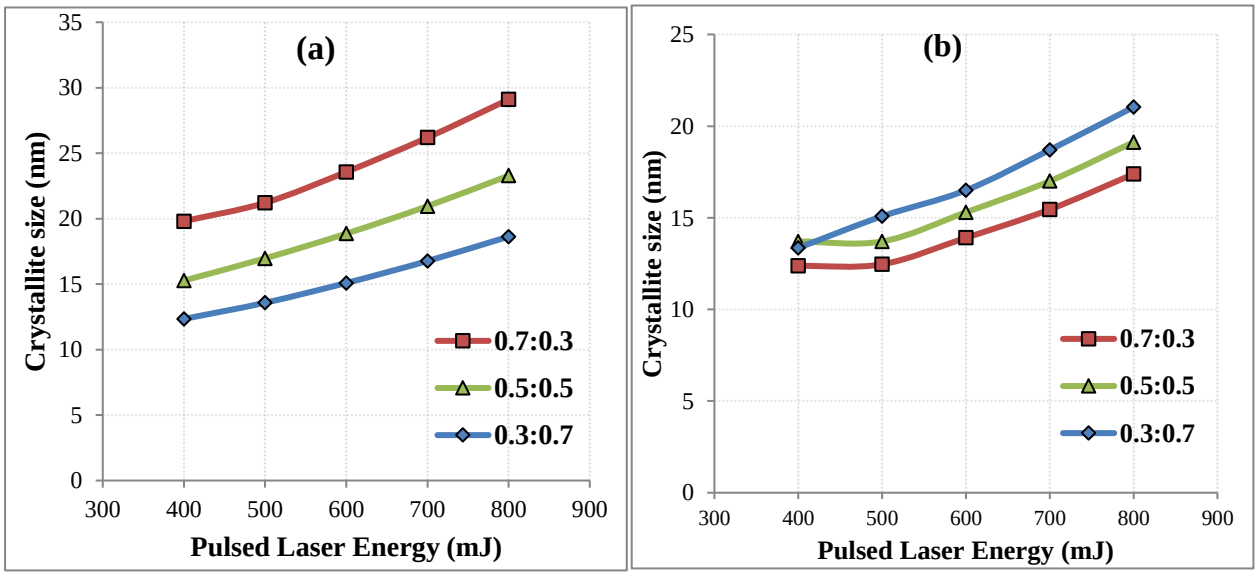

Figure 14: variation of crystallite size with laser energy calculated using the Scherrer formula of (a) copper and (b) aluminum crystals from different composition ratios of the started targets

Fig. 15 displays the correlation of the crystallite size of CuNPs and AlNPs with plasma temperature from Cu: Al targets of the different composition ratios. The higher electron temperature means more energy is transferred to the plasma, which leads to more interaction

between the laser- induced plasma and the target material. This can cause the target material to vaporize more effectively, producing more highly energetic atoms and ions. Increasing electron temperature in the plasma induced by pulsed laser significantly affects the crystallite size of the generated nanoparticles, especially at the highest temperature [25]. The crystallite size was increased with the increase in plasma temperature. The created seed particles inside plasma may be heated by collisions with electrons. The collected positive charge nanoparticles attract free electrons and increase the frequency of electron-cluster collisions according to plasma density. These electrons act as a heating source during the growth of the clusters, delaying the cooling process by the surrounding plasma, which leads to further development of the particles and enhancing crystallization [25].

On the other hand, Cu's crystallite size is greater than Al's at all laser energies for $Cu_{0.7}$:$Al_{0.3}$ and $Cu_{0.5}$:$Al_{0.5}$ and be opposite at $Cu_{0.3}$:$Al_{0.5}$. The difference in crystallite size of the two elements in the composite nanoparticles not depend only on their existence in the target but on the pulsed laser energy as a result of different capability of laser interaction with the different element.

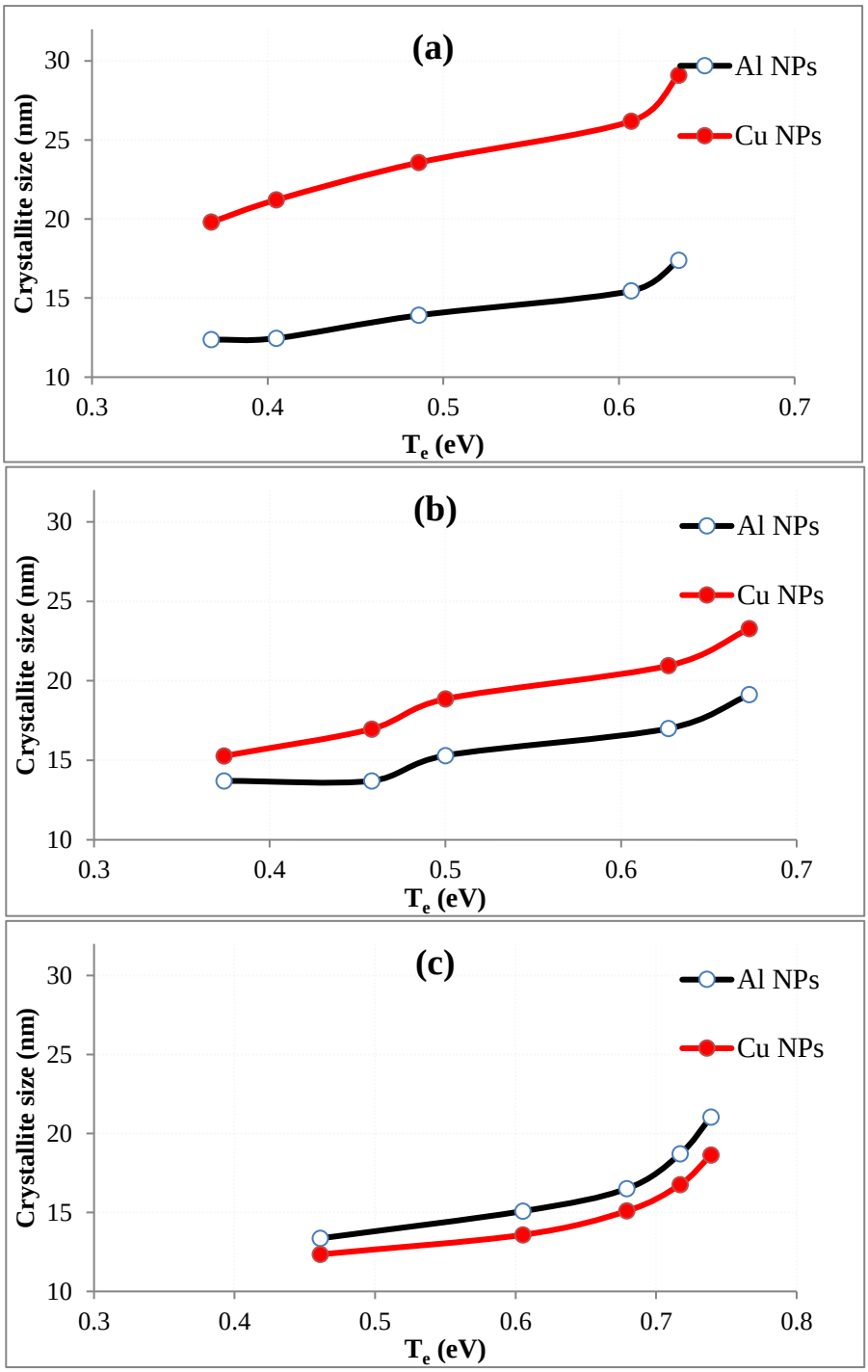

Figure 15: correlation of crystallite size CuNPs and AlNPs with plasma temperature from the target of different Cu: Al composition ratios (a) $Cu_{0.7}$:$Al_{0.3}$, (b) $Cu_{0.5}$:$Al_{0.5}$, and (c) $Cu_{0.3}$:$Al_{0.7}$.

4. Conclusions

The effects of laser energy and target composition on plasma characteristics, as well as their correlation with the crystallite size of the ablated nanoparticles, were investigated. When studying plasma emission induced by laser irradiation, both the pulsed laser's energy and the target material's composition should be considered. The work function of the metals involved significantly determines the intensity and ratio of emission lines observed in the resulting plasma induced by pulsed laser irradiation. The laser photons extracted electrons from the metal surface, according to them, to work function and exhibit stronger plasma emission. The emission line intensities reflect the dynamics of collisions. The intensity ratio variation for the selected emission lines, Al-I (309.27 nm)/Cu-I (324.75 nm), responds to changes in the pulsed laser energy and the

Cu:Al target ratio. It is observed that all ratios are greater than unity, especially at low laser energies. At lower laser energies, the difference in work functions becomes more pronounced. Both Te and ne values show a direct increase from the pulsed laser energy. The elevation of electron temperature and density causes a low cooling process by the environment after ablation, leading to increased growth and the formation of larger crystallites with higher crystallinity. More electrons in one area cause more collisions between electron clusters, which helps the nanoparticles to crystallize better. This knowledge benefits in controlling the nanoparticles crystallinity by adjusting plasma behaviour.

Conflict of interest

The authors declare that they have no conflict of interest.

References

1. R.S. Mohammed, K.A. Aadim, and K.A. Ahmed. Karbala Int. J. Mod. Sci. **8**(2), 88–97 (2022). https://doi.org/ 10.33640/2405-609X.3225.
2. V. Unnikrishnan, K. Alti, V. Kartha, C. Santhosh, G. Gupta, and B. Suri. Pramana - J. Phys. **74**, 983 (2010). https:// 10.1007/s12043-010-0089-5.
3. R.J.E. Jaspers. Fusion Sci. Technol. **61**, 384 (2012). https://doi.org/ 10.33640/2405-609X.3225.
4. A. Ajith, M.N.S. Swapna, H. Cabrera, and S.I. Sankararaman. Photonics. **10**, (2023). https://doi.org/ 10.3390/photonics10020199 .
5. S.T. Hsieh, H. Mishra, N. Bolouki, W. Wu, C. Li, and J.-H. Hsieh. Coatings. **12**, 1014 (2022). https:// 10.3390/coatings12071014..
6. K.A. Aadim, A.A. Hussain, and M.R. Abdulameer. Iraqi J. Phys. **12**, 97 (2014). https://doi.org/10.30723/ijp.v12i23.344.
7. A. Sergievskaya, A. O'Reilly, A. Chauvin, J. Veselý, A. Panepinto, J. De Winter, D. Cornil, J. Cornil, and S. Konstantinidis. Colloids Surfaces A Physicochem. Eng. Asp. **615**, 126286 (2021). https://doi.org/ 10.1016/j.colsurfa.2021.126286.
8. S.Z. Wu. J. Appl. Phys. **98**(8) (2005). https://doi.org/10.1063/1.2112177.
9. A. Ojeda-G-P, M. Döbeli, and T. Lippert. Adv. Mater. Interfaces. **5**, 1 (2018). https:// 10.1002/admi.201701062
10. M. Šícha, Z. Hubicka, L. Soukup, L. Jastrabík, M. Cada, and P. Špatenka. Surf. Coatings Technol. **148**, 199 (2001). https:// 10.1016/S0257-8972(01)01338-X.
11. R.K. Jamal, K.A. Aadim, Q.G. Al-Zaidi, and I.N. Taaban. Photonic Sensors. **5**, 235 (2015). https://doi.org/10.1007/s13320-015-0253-0.
12. Online Available- http://kinetics.nist.gov/index.php. (2025). https:// doi.org/kinetics.nist.gov/index.php.
13. K.A. Aadim, and R.H. Jassim. AIP Conf. Proc. **2372**, 080014 (2021). https://doi.org/10.1063/5.0067300.
14. Bolouki, Hsieh, Li, and Yang. Plasma. **2**, 283 (2019). https://doi.org/10.3390/plasma2030020.
15. R. Wang, C. Yang, J. Hao, J. Shi, F. Yan, N. Zhang, B. Jiang, and W. Shao. Coatings. **12**, 394 (2022). https://doi.org/10.3390/coatings12030394.
16. M. Stössel, J. Staudigel, F. Steuber, J. Simmerer, and A. Winnacker. Appl. Phys. A Mater. Sci. Process. **68**, 387 (1999). https://doi.org/10.1007/s003399900011.
17. A. Kiejna, and K.F. Wojciechowski. [Internet]. In: *Metal Surface Electron Physics*, Elsevier, 123 (1996). https://doi.org/10.1016/B978-008042675-4/50009-8.
18. M.T. Hussein, K.A. Aadim, and E.K. Hassan. Adv. Mater. Phys. Chem. **06**, 85 (2016). https://doi.org/ 10.4236/ampc.2016.64009.
19. A. Alwen, and A.M. Hodge. Mater. Res. Express. **10**, 016402 (2023). https://doi.org/10.1088/2053-1591/acb31a.
20. J.-X. Zhang, and Z.-Y. Zhao. Mater. Sci. Semicond. Process. **167**, 107819 (2023). https://doi.org/10.1016/j.mssp.2023.107819.
21. R. Bo, N. Nasiri, H. Chen, D. Caputo, L. Fu, and A. Tricoli. ACS Appl. Mater. Interfaces. **9**, 2606 (2017). https://doi.org/10.1021/acsami.6b12321.
22. H.J. Imran, K.A. Hubeatir, K.A. Aadim, and D.S. Abd. J. Phys. Conf. Ser. **1818**, (2021). https://doi.org/10.1088/1742-6596/1818/1/012127.
23. 24. N. Hellgren, K. Macák, E. Broitman, M.P. Johansson, L. Hultman, and J.E. Sundgren. J. Appl. Phys. **88**, 524 (2000). https://doi.org/10.1063/1.373690.
25. F. Taccogna, M. Dell'Aglio, M. Rutigliano, G. Valenza, and A. De Giacomo. Plasma Sources Sci. Technol. **26**, 045002 (2017). https://doi.org/10.1088/1361-6595/aa595b.

حساب معاملات البلازما لـ ($Cu_{1-x}:Al_x$) المحضرة بواسطة البلازما المستحثة بالليزر: تأثير طاقات الليزر

نوفل علي نوري[1] وكاظم عبدالواحد عادم[1]و سلام محمد
[1]قسم الفيزياء، كلية العلوم، جامعة بغداد، بغداد، العراق
[2]قسم الهندسة الكيميائية والبترولية، كلية الهندسة والزراعة، جامعة نزوى، سلطنة عمان

الخلاصة

يتناول هذا البحث دراسة العلاقة بين معلمات البلازما المُستحثة بواسطة الليزر النبضي من أهداف النحاس – ألومنيوم ($Cu_{1-x}:Al_x$) عند نسب مختلفة ($x = 0.3$ و0.5 و 0.7) وخصائص الجسيمات النانوية المُستأصلة. تُظهر النتائج زيادة في كثافة عدد الإلكترونات (n_e) ودرجة حرارة البلازما (T_e) مع زيادة طاقة الليزر النبضي ونسبة الهدف. زاد حجم بلورات النحاس والألمنيوم في الجسيمات النانوية المركبة مع درجة حرارة البلازما (من 12.4 إلى 17.4 نانومتر، ومن 13.7 إلى 19.1 نانومتر، ومن 13.4 إلى 21.0 نانومتر لبلورات الألومنيوم، بينما زاد من 19.8 إلى 29.1 نانومتر، ومن 15.3 إلى 23.3 نانومتر، ومن 12.3 إلى 18.6 نانومتر لبلورات النحاس للنسب ($x = 0.3$ و 0.5 و 0.7). كلما زادت قيمة T_e، زادت الطاقة المنقولة إلى البلازما، مما يعزز عملية الاستئصال. أدت زيادة T_e إلى زيادة كبيرة في حجم بلورات الجسيمات النانوية الناتجة، وخاصة عند أعلى درجة حرارة. يمكن تسخين جزيئات الاولية الناتجة داخل البلازما عن طريق التصادمات مع الإلكترونات، والتي تعمل كمصدر تسخين أثناء نمو العناقيد، مما يعزز التبلور. حجم بلورات النحاس أكبر من حجم بلورات الألومنيوم عند جميع طاقات الليزر من $Cu_{0.7}:Al_{0.3}$ و$Cu_{0.5}:Al_{0.5}$، ويكون معاكسًا في عينة $Cu_{0.3}:Al_{0.7}$. يعتمد اختلاف حجم بلورات العنصرين في الجسيمات النانوية المركبة على نسبة وجودهما في الهدف وعلى طاقة الليزر النبضي، نتيجةً لاختلاف قدرة تفاعل الليزر مع العناصر المختلفة. يمكن استخدام هذه النتائج لتحسين عمليات الاستئصال لإنتاج جسيمات نانوية للعديد من التطبيقات العلمية. وجدت هذه الدراسة علاقة بين معلمات البلازما المستحثة وحجم بلورات الجسيمات النانوية المستأصلة.

الكلمات المفتاحية: PLA، خصائص البلازما، مطيافية انبعاث البلازما، جسيمات النانو نحاس:ألمنيوم، الخواص التركيبية.